International Journal of Applied Electromagnetics and Mechanics 00 (2014) 1–11 1
DOI 10.3233/JAE-141748
IOS Press

Comparison of particle swarm optimization and self-adaptive dynamic differential evolution for the imaging of a periodic conductor

Yu-Ting Cheng, Chien-Ching Chiu*, Shuo-Peng Chang and Jung-Chin Hsu
Electrical Engineering Department, Tamkang University Tamsui, Taiwan

Abstract. The application of two techniques to reconstruct the shape of a two-dimensional periodic perfect conductor from mimic the measurement data is presented. A periodic conducting cylinder of unknown periodic length and shape scatters the incident wave in half-space and the scattered field is recorded outside. After an integral formulation, the microwave imaging is recast as a nonlinear optimization problem; a cost functional is defined by the norm of a difference between the measured scattered electric fields and the calculated scattered fields for an estimated shape of a conductor. Thus, the shape of conductor can be obtained by minimizing the cost function. In order to solve this inverse scattering problem, transverse magnetic (TM) waves are incident upon the objects and two techniques are employed to solve these problems. The first is based on an particle swarm optimization (PSO) and the second is a self-adaptive dynamic differential evolution (SADDE). Both techniques have been tested in the case of simulated mimic the measurement data contaminated by additive white Gaussian noise. Numerical results indicate that the SADDE algorithm is better than the PSO in reconstructed accuracy and convergence speed.

Keywords: Inverse scattering, frequency-domain, self-adaptive dynamic differential evolution, particle swarm optimization

1. Introduction

The detection and reconstruction of buried and inaccessible scatterers by inverting microwave electromagnetic data is a research field of considerable interest because of numerous applications in geophysical prospecting, civil engineering, and nondestructive testing. Numerical inverse scattering studies found in the literature are based on either frequency or time domain approaches. However, it is well known that one major difficulty of inverse scattering is its ill-posedness in nature [1].

Another inverse scattering problem is the nonlinearity because it involves the product of two unknowns: the electrical property of object, and the electric field within the object. In general, the nonlinearity of the problem is coped with by applying iterative optimization techniques [2,3]. These algorithms based on stochastic strategies, offer advantages relative to local inversion algorithms including strong search ability, simplicity, robustness, and insensitivity to ill-posedness. In contrast to traditional computation systems, evolutionary computation [4–8] provides a more robust and efficient approach

*Corresponding author: Chien-Ching Chiu, Electrical Engineering Department, Tamkang University Tamsui, Taiwan. E-mail: chiu@ee.tku.edu.tw.

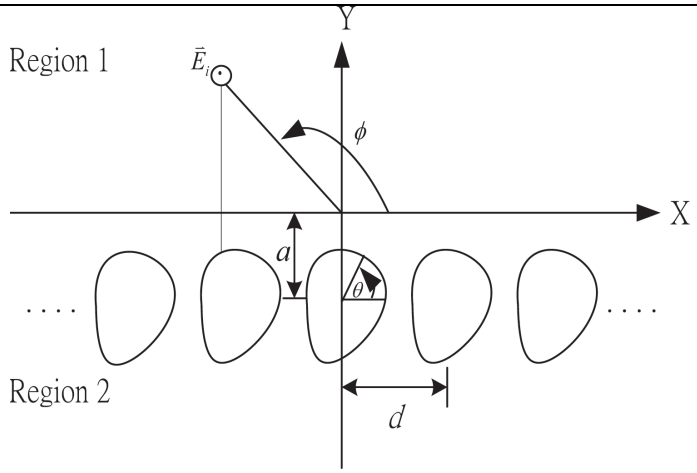

Fig. 1. Geometry of the problem in (x, y) plane.

for solving inverse scattering problems. Particle swarm optimization (PSO) has proven to be a useful method of optimization for difficult and discontinuous multidimensional engineering problems [9,10]. PSO is very efficient at exploring the entire search space. A new method of optimization, Self-Adaptive dynamic differential evolution (SADDE) is able to accomplish the same goal as genetic algorithm (GA) optimization in a new and faster way. Since PSO and SADDE both work with a population of solutions, combining the searching abilities of both methods seems to be a good approach.

Frequency domain inverse scattering by population-based stochastic algorithms are published in the last ten years. Concerning the shape reconstruction of conducting scatterers, the PSO has been investigated whereas the GA has been utilized in the reconstruction of periodic conductor scatterers [11,12]. In this case, the reported results indicate that the PSO is reliable tools for inverse scattering applications. Moreover, it has been shown that both DE and PSO outperform real-coded GA in terms of convergence speed. In recent decade years, some papers have compared different algorithm in inverse scattering [4]. However, to our knowledge, a comparative study about the performances of particle swarm optimization and self-adaptive dynamic differential evolution when applied to inverse scattering problems of a periodic conductor has not yet been investigated .

In this paper, the inverse scattering problem of a periodic perfectly conducting cylinder by transverse magnetic(TM) wave illumination is investigated on the application of both PSO and SADDE. In section II, the solution of the forward scattering problem is presented. In section III and IV, inverse problem and the numerical results of the proposed inverse problem are given, respectively. Section V gives the conclusions.

2. Forward problem

Let us consider a periodic cylinder which is partially immersed in a lossy homogeneous half-space, as shown in Fig. 1 Media in regions 1 and 2 are characterized by permittivities and conductivities $(\varepsilon_1, \sigma_1)$ and $(\varepsilon_2, \sigma_2)$ respectively. A perfectly conducting cylinder is illuminated by a TM plane wave. The array is periodic in the x-direction with a periodic length d and is uniform in the z-direction. The cross-section is described in polar coordinates in the x, y plane by the equation $\rho = F(\theta)$. We assume that the time

dependence of the field is harmonic with the factor $e^{j\omega t}$. Let $\overrightarrow{E}^{inc}$ denote the incident field form region 1 with incident angle ϕ as shown in Fig. 1. The scattered field, $\vec{E}_s = E_s\hat{z}$ can be expressed by

$$E_s(x,y) = \int_0^{2\pi} G(x,y;x,y')J(\theta')d\theta' \tag{1}$$

Where

$$G(x,y;x',y') = \begin{cases} G_1(x,y;x',y'), y \leqslant -a \\ G_2(x,y;x',y'), y > -a \end{cases} \tag{2}$$

$$G_1(x,y;x',y') = \sum_{l=-\infty}^{\infty} \frac{1}{2\pi} \int_{-\infty}^{\infty} \frac{j}{\gamma_1+\gamma_2} e^{j\gamma_1(y+a)} e^{-j\gamma_2(y'+a)} e^{-j\alpha(x-x'-ld)} d\alpha \tag{3}$$

$$G_2(x,y;x',y') = \sum_{l=-\infty}^{\infty} \frac{1}{2\pi} \int_{-\infty}^{\infty} \frac{j}{2\gamma_2} \left(e^{-j\gamma_2|y-y'|} + \frac{\gamma_2-\gamma_1}{\gamma_2+\gamma_1} e^{-j\gamma_2(y+2a+y')} \right) e^{-j\alpha(x-x'-ld)} d\alpha \tag{4}$$

$$J(\theta) = -j\omega\mu_0\sqrt{F^2(\theta)+F'^2(\theta)}J_s(\theta) \tag{5}$$

With

$$\gamma_q^2 = k_q^2 - \alpha^2, k_q^2 = \omega^2\mu_0\varepsilon_q - j\omega_0\sigma_q, q = 1,2$$

Here $G(x,y;x',y')$ is the two-dimensional half-space periodic Green's function, and J_s (θ) is the induced surface current density which is proportional to the normal derivative of electric field on the conductor surface. a is buried depth. The boundary condition at the surface of the scatterer states that the total tangential electric field must be zero and this yield an integral equation for $J(\theta)$:

$$E_i(F(\theta),\theta) = -\int_0^{2\pi} G(x,y,x',y')J(\theta')d\theta' \tag{6}$$

For the direct scattering problem, the scattered field E_s is calculated by assuming that the periodic length d and the shape function $F(\theta)$ of the object is known. This can be achieved by first solving J(θ) in Eq. (6) and calculating E_s in Eq. (1). For numerical calculation of the direct problem, the contour is first divided into sufficient small segments so that the induced surface current can be considered constant over each segment. Then the moment method is used to solve Eqs (6) and (1) with pulse basis function for expanding and Dirac delta function for testing. Note that, for numerical implementation of the periodic Green's function, we might face some difficulties in calculating this function. In fact, when y approaches y', the infinite series in Eq. (3), Eq. (4) is very poor convergent. Fortunately, the infinite series may be rewritten as a rapidly convergent series plus an asymptotic series which can be summed efficiently. Thus the infinite series in the periodic Green's function can be calculated efficiently [11–16].

For the inverse problem, assume the approximate center of scatterer, which in fact can be any point inside the scatterer, is known. Then the shape function $F(\theta)$ can be expanded as:

$$F(\theta) = \sum_{n=0}^{N/2} B_n\cos(n\theta) + \sum_{n=1}^{N/2} C_n\sin(n\theta) \tag{7}$$

where B_n and C_n are real coefficients to be determined, and $N+1$ is the number of unknowns for the shape function. In the inversion procedure, the PSO and SADDE are used to minimize the following objective function:

$$OF = \left\{ \frac{1}{M_t} \sum_{m=1}^{M_t} \left| E_s^{\exp}(\bar{r}_m) - E_s^{cal}(\bar{r}_m) \right|^2 / \left| E_s^{\exp}(\bar{r}_m) \right|^2 \right\}^{1/2} \tag{8}$$

where M_t is the total number of the mimic measurement data points. $E_s^{\exp}(\vec{r}_m)$ and $E_s^{cal}(\vec{r}_m)$ are the measured and calculated scattered fields, respectively.

3. Inverse problem

3.1. Particle swarm optimization

Particle swarm global optimization is a class of derivative-free, population-based and self-adaptive search optimization technique which introduced by Kennedy and Eberhart [3]. Particles are distributed throughout the searching space and their positions and velocities are modified based on social behavior. The social behavior in PSO is a population of particles moving towards the most promising region of the search space. Clerc [17] proposed the constriction factor to adjust the velocity of the particle for obtaining the better convergence; the algorithm was named as constriction factor method.

PSO starts with an initial population of potential solutions that is composed by a group of randomly generated individuals representing shape function of the cylinder. After the initialization step, each particle of population has assigned a randomized velocity and position. Thus, each particle has a position and velocity vector, and moves through the problem space. In each generation, the particle changes its velocity by its best experience, called x_{pbest}, and that of the best particle in the swarm, called x_{gbest}. Assume there are N_p particles in the swarm that is in a search space in D dimensions, the position and velocity could be determine according to the following equations (constriction factor method):

$$v_{ij}^g = w \cdot v_{ij}^{g-1} + c_1 \cdot \varphi_1 \cdot \left(X_{pbest_{ij}}^g - x_{ij}^{g-1} \right) + c_2 \cdot \varphi_2 \cdot \left(X_{gbest_{ij}}^g - x_{ij}^{g-1} \right) \tag{9}$$

$$x_{ij}^g = x_{ij}^{g-1} + v_{ij}^g \tag{10}$$

where v_{ij}^g and x_{ij}^g are the velocity and position of the i-th particle in the j-th dimension at g-th generation, φ_1 and φ_2 are both the random number between 0 and 1, c_1 and c_1 are learning coefficients and w is the inertial weighting factor that can avoid the particle trapped into the local minimized solution.

It should be noted that the shape function used to describe the shape of the cylinder will be determined by the PSO scheme. The flowchart of the PSO is shown in Fig. 2. PSO goes through five procedures as follows:

1. Initialize a starting population: Randomly generate a swarm of particles.
2. Calculate E fields.
3. Evaluate the population using objective function: The PSO algorithm evaluates the objective function Eq. (8) for each individual in the population.
4. Find x_{pbest} and x_{gbest}.
5. Update the velocity and position.

Stop the process and print the best individual if the termination criterion is satisfied, else go to step II.

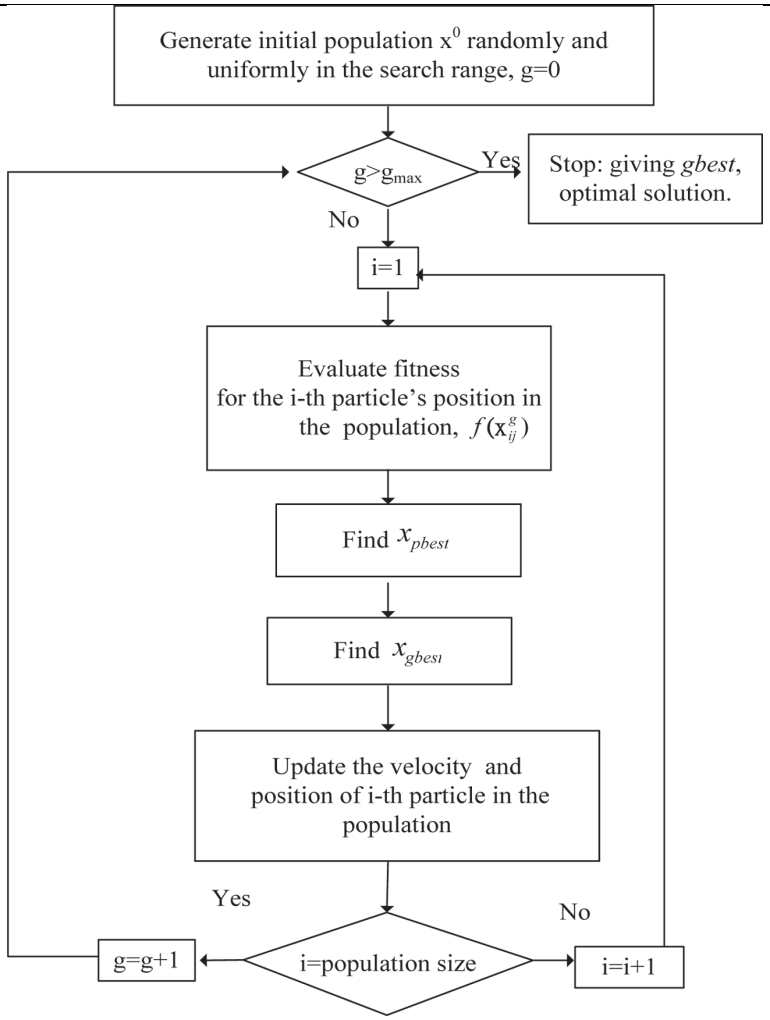

Fig. 2. Flowchart for the particle swarm optimization (PSO).

3.2. Self-Adaptive Dynamic Differential Evolution (SADDE)

The SADDE are based on DDE scheme. The SADDE algorithm starts with an initial population of potential solutions that is composed by a group of randomly generated individuals which represents periodic length and the shape function of the cylinders. The flowchart of the SADDE algorithm is shown in Fig. 3. SADDE algorithm goes through six procedures as follows:

1. Initialize a starting population: Individuals in SADDE algorithm represent a set of D-dimensional vectors in the parameter space for the problem, $\{X_i : i = 1, 2, \cdots, Np\}$, where D is the number of parameters to be optimized and *Np* is the population size.
2. Evaluate the population using cost function: After initialization, SADDE algorithm evaluates the objective function Eq. (8) for each individual in the population.
3. Perform mutation operation to generate trial vectors: The mutation operation of SADDE algorithm is performed by arithmetical combination of individuals. For each parameter vector X_i of the parent

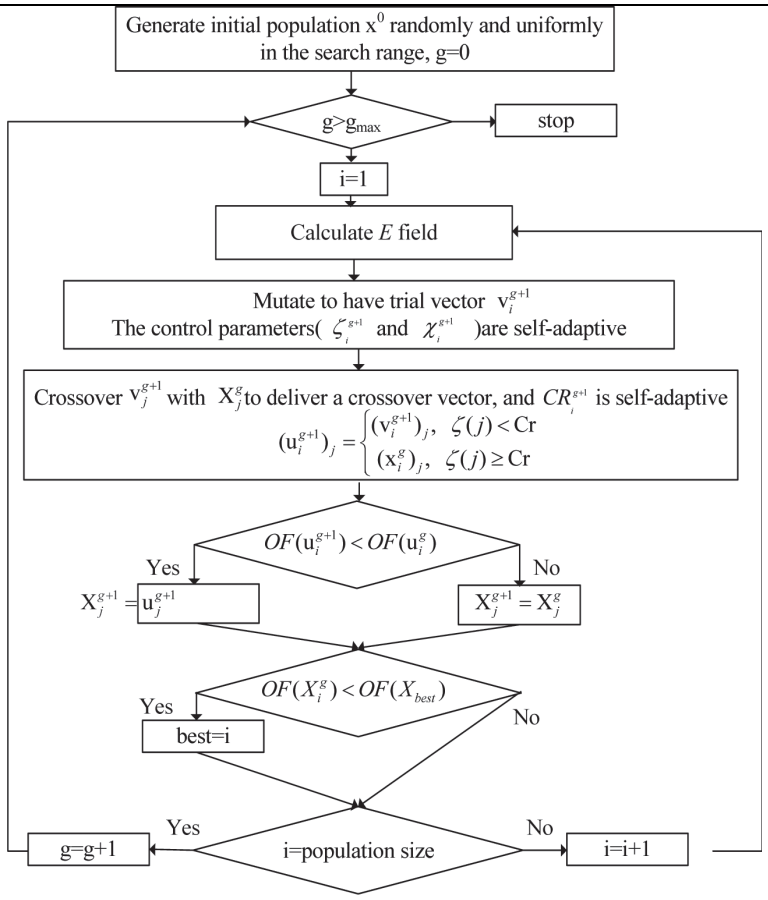

Fig. 3. Flowchart for the self-adaptive dynamic differential evolution (SADDE).

generation, a trial vector V_i is generated according to the following equation:

$$(V_i^{g+1})_j = (X_i^g)_j + \xi \cdot [(X_{\text{best}}^g)_j - (X_i^g)_j] + \chi \cdot [(X_m^g)_j - (X_n^g)_j],$$
$$m, n \in [0, N_p - 1], m \neq n \tag{11}$$

where ξ and χ are the scaling factors associated with the vector differences $(X_{best}^g - X_i^g)$ and $(X_m^g - X_n^g)$, respectively. The disturbance vector V due to the mutation mechanism consists of parameter vector X_i^g, the best particle X_{best}^g and two randomly selected vectors. Note that ξ and χ are adjusted automatically.

In SADDE, The basic idea is to have the control parameters evolve through generations. New vectors are generated by using the evolved values of the control parameters. These new vectors are more likely to survive and produce offspring during the selection procedure. In turn, the survived vectors carry the improved values of the control parameters to the next generation. Therefore, the control parameters are self-adjusted in every generation for each individual according to the following scheme:

$$\xi_i^{g+1} = \begin{cases} \xi_l + \mathit{rand}_1 * \xi_u, & \text{if } \mathit{rand}_2 < 0.1 \\ \xi_i^g, & \text{otherwise} \end{cases} \tag{12}$$

$$\chi_i^{g+1} = \begin{cases} \chi_l + \ \textit{rand}_3 * \chi_u, & \text{if} \quad \textit{rand}_4 < 0.1 \\ \chi_i^g, & \text{otherwise} \end{cases} \tag{13}$$

where *rand1*, *rand2*, *rand3* and *rand4* are random numbers with the values uniformly distributed between 0 and 1. ξ_l, ξ_u, χ_l and χ_u are the lower and the upper limits of ξ and χ, respectively .Both ξ_l and χ_l are set to 0.1 and both ξ_u and $\chi_u$are set to 0.9 [18,19].

4. Perform crossover operation with probability of crossover *CR* to deliver crossover vectors: The crossover operation of SADDE algorithm is performed to increase the diversity of the parameter vectors. This operation is similar to the crossover process in GAs. However, the crossover operation of SADDE algorithm just allows to deliver the crossover vector u_i by mixing component of the current vector X_i^g and the trial vector V_i. It can be expressed as:

$$(u_i^{g+1})_j = \begin{cases} (\mathrm{V}_i^{g+1})_j, \ \zeta(j) < \mathrm{Cr} \\ (\mathrm{X}_i^g)_j, \ \zeta(j) \geqslant \mathrm{Cr} \end{cases} \tag{14}$$

$$\mathrm{Cr}_i^{g+1} = \begin{cases} \textit{rand}_5, & \text{if} \quad \textit{rand}_6 < 0.1 \\ \mathrm{Cr}_i^g, & \text{otherwise} \end{cases} \tag{15}$$

where Cr is the probability of crossover, $Cr \in (0, 1)$. *rand5* and *rand6* are random numbers with the values uniformly distributed between 0 and 1. $\zeta(j)$ is the random number generated uniformly between 0 and 1.

5. Perform selection operation to produce offspring: Selection operation is conducted by comparing the parent vector X_i^g with the crossover vectors u_i^{g+1}. The vector with smaller cost function value is selected as a member of the next generation. Explicitly, the selection operation for the minimization problem is given by:

$$\mathrm{X}_i^{g+1} = \begin{cases} u_i^{\mathrm{g+1}}, & \text{if } \textit{OF}\,(u_i^{g+1}) < \textit{OF}\,(X_i^g) \\ \mathrm{X}_i^g, & \text{otherwise} \end{cases} \tag{16}$$

The SADDE algorithm is carried out in a dynamic way: each parent individual will be replaced by his offspring if the offspring has a better cost function value than its parent individual does.

6. Stop the process and obtain the best individual if the termination criterion is satisfied, else go to step 2.

The algorithm of SADDE is a self-adaptive version of DDE, which is processed of self-adaptibility and the ability of approaching the "Best". Based on the self-adaptive concept, the parameters ξ, χ and Cr adjust automatically while the time complexity does not increase.

4. Numerical results

We illustrate the performance of the proposed inversion algorithm and its sensitivity to random noise in the scattered field. Let us consider a perfectly conducting cylinder buried in a lossless half-space ($\sigma_1 = \sigma_2 = 0$). The permittivity in each region is characterized by $\varepsilon_1 = \varepsilon_0$ and $\varepsilon_2 = 2.56\varepsilon_0$ respectively. The frequency of the incident wave is chosen to be 1 GHz with incident angles ϕ equal to 45°, 90° and 135°, respectively. The wavelength λ_0 is 0.1 m. For each incident wave, 18 measurements are made at the points equally separated on a semi-circle with the radius of 2.1 m in region 1. There are 54 measurement points in each simulation. We set the total number of generation to be 500 (i.e., $\mathrm{g}_{\max} = 500$), c_1 and c_2 to be 1.3 and 2.8 respectively. The population size is chosen as 35. Number of unknowns is set to be 8 (i.e., N + 2 = 8), In other words, seven unknowns for the shape function $F(\theta)$ and one unknowns for

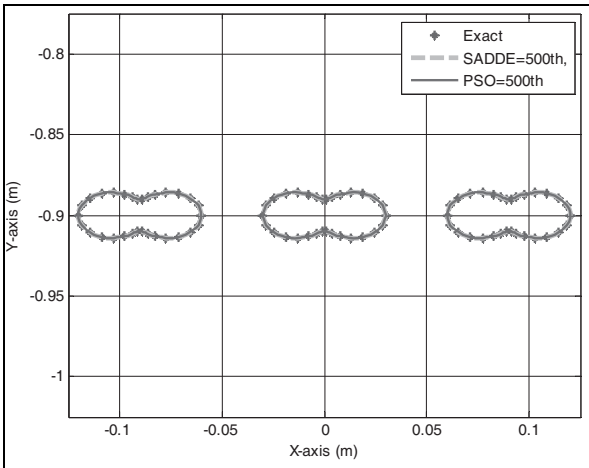

Fig. 4. The reconstructed shape of the cylinder for example 1.

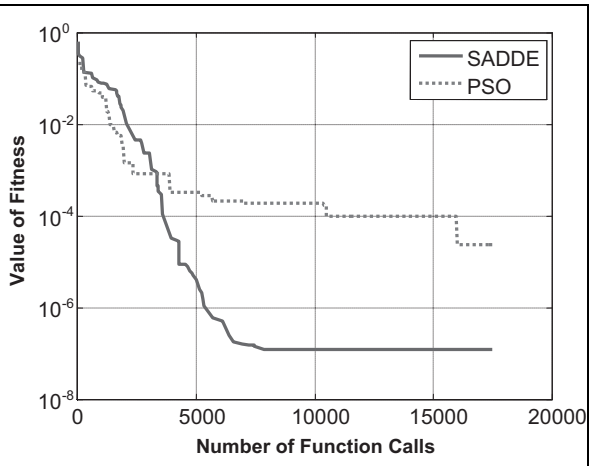

Fig. 5. The value of fitness versus the number of function calls for example 1.

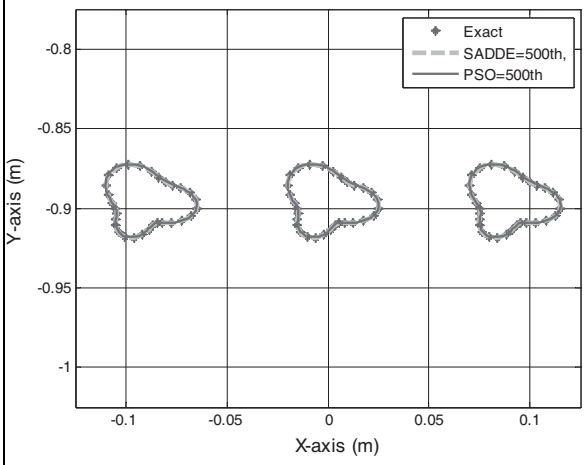

Fig. 6. The reconstructed shape of the cylinder for example 2.

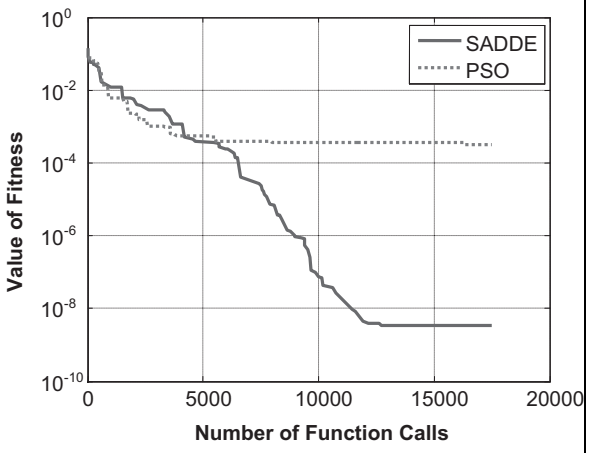

Fig. 7. The value of fitness versus the number of function calls for example 2.

period length. The search range for the unknown coefficient of the shape function is chosen to be from 0 to 0.1. The search range for the unknown periodic length is chosen from 0.05 to 0.1. Our purpose is to reconstruct the shape of the object by using the scattered field at different incident angles.

Three examples are investigated for the inverse scattering of the proposed structure by using the PSO and SADDE. In the first example, the shape function is chosen to be $F(\theta) = (0.02+0.01\cos 2\theta)$ m. The reconstructed shape function of PSO and SADDE for the best population member is plotted in Fig. 4 and the value of fitness versus the number of function calls for example 1 is shown in Fig. 5. The number of function calls is the number of the calculation of direct problem. The total number of function calls is the total generations multiply by population size. The reconstructed shape error by PSO and SADDE are 0.4% and 0.1%, respectively. It is clear that the reconstructed result is good.

In the second example, the shape function is chosen to be $F(\theta) = (0.02 + 0.005\cos 3\theta + 0.005\sin\theta)$ m. This example shows that the proposed scheme can reconstruct more complicated scatterer whose

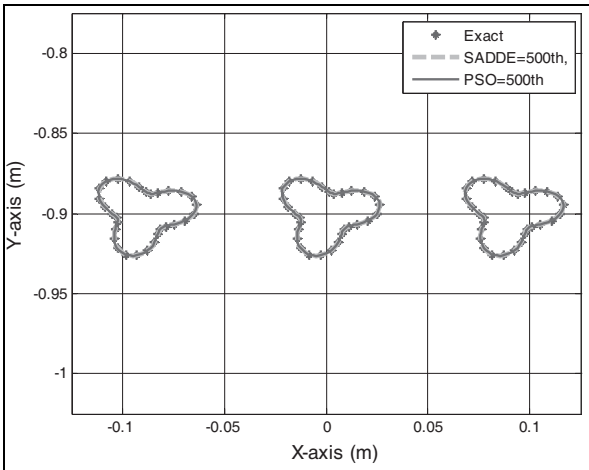

Fig. 8. The reconstructed shape of the cylinder for example 3.

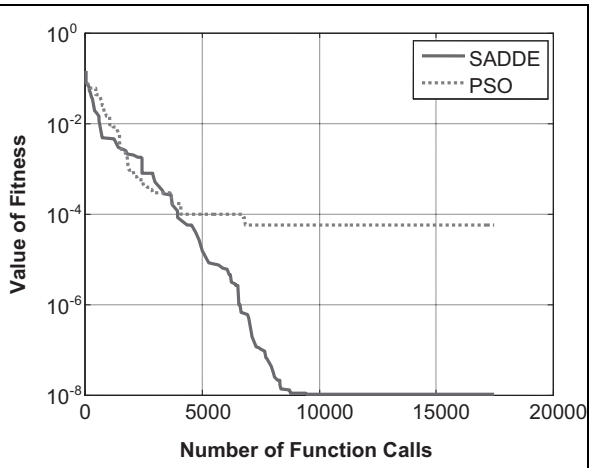

Fig. 9. The value of fitness versus the number of function calls for example 3.

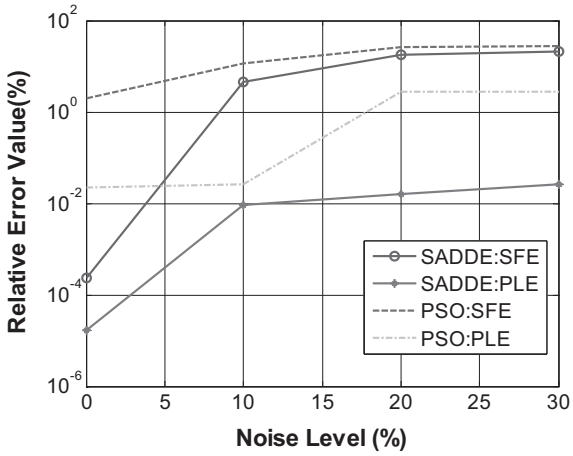

Fig. 10. Shape function error and periodic length error as functions of noise level by PSO and SADDE.

shape function has three concavities. The reconstructed shape function for the best population member is plotted in Fig. 6 and the value of fitness versus the number of function calls for example 2 is shown in Fig. 7. The reconstructed shape error by PSO and SADDE are 1.33% and 0.62%, respectively. There is a small discrepancy in the bottom of the shape since TM waves are incident from the top of the shape.

In the third example, the shape function is chosen to be $F(\theta) = (0.02+0.005\cos 3\theta+0.005\sin 3\theta)$m. The reconstructed shape function for the best population member is plotted in Fig. 8 and the value of fitness versus the number of function calls for example 3 is shown in Fig. 9. The reconstructed shape error by PSO and SADDE are 2.03% and 0.6%, respectively. It is seen that the error comes from the bottom of the shape, but we still can obtain good results by PSO algorithm and SADDE.

From the three example, it is observed that PSO converges faster when the number of function calls are less than 5000. However, SADDE can get more accurate results when the number of function calls became large. As a result, SADDE are better then PSO for the complex objects. To investigate the effects of noise, we add to each complex scattered field a quantity $b+cj$, where b and c are independent random

numbers having a uniform distribution over 0 to the noise level times the R.M.S value of the scattered field. Normalized standard deviations of 10%, 20% and 30%, respectively, are used in the simulations. Figure 10 shows the reconstructed results under the condition that the scattered E fields to mimic the measurement data contaminated by the noise. The discrepancy of shape function of the reconstructed shape is shown in Fig. 10. Here *PLE* and *SFE*, which are called periodic length error and shape function discrepancies, respectively, are defined as

$$PLE = \frac{\left|d^{cal} - d\right|}{d} \tag{17}$$

$$SFE = \left\{ \frac{1}{N'} \sum_{i=1}^{N'} [F^{cal}(\theta_i) - F(\theta_i)]^2 / F^2(\theta_i) \right\}^{1/2} \tag{18}$$

where N' is set to 100. Quantities *PLE* and *SFE* provide measures of how well d^{cal} approximates d and $F^{cal}(\theta)$ approximates $F(\theta)$, respectively. It could be observed that good reconstruction has been obtained for shape of the perfectly conducting cylinder when the relative noise level is below 10%.

5. Conclusion

The problems of the periodic length and shape reconstruction of periodic conducting cylinder are investigated. Based on the boundary condition and the measured scattered field, we have derived a set of nonlinear integral equations and reformulated the imaging problem into an optimization one which solved by applying SADDE and PSO techniques.

The objective function of both PSO and SADDE is to minimize the discrepancy between measured and estimated scattered field data. Numerical results show that SADDE outperforms the PSO in terms of accuracy and convergence speed, when the same number of iterations is applied, since SADDE realizes the ideas of approaching the "Self-Adaptive". SADDE algorithm can result in accurate reconstruction even when the effects of noise are included under the condition of noise level less than 10^{-2}.

References

[1] P.C. Sabatier, Theoretical Considerations For Inverse Scattering, *Radio Science* **18** (Jan. 1983), 629–631.
[2] R. Storn and K. Price, Differential Evolution – a Simple and Efficient Adaptive Scheme for Global Optimization over Continuous Spaces, Technical Report TR-95-012, International Computer Science Institute, Berkeley, 1995.
[3] J. Kennedy and R.C. Eberhart, Particle Swarm Optimization, *Proceedings of the IEEE International Conference on Neural Network*, 1995, pp. 1942–1948.
[4] I.T. Rekanos, Shape Reconstruction of a Perfectly Conducting Scatterer Using Differential Evolution and Particle Swarm Optimization, *IEEE Transactions on Geoscience and Remote Sensing* **46**(7) (2008), 1967–1974.
[5] A. Semnani and M. Kamyab, An Enhanced Method for Inverse Scattering Problems Using Fourier Series Expansion in Conjunction with FDTD and PSO, *Progress In Electromagnetic Research* **PIER 76** (2007), 45–64.
[6] A. Semnani, M. Kamyab and I.T. Rekanos, Reconstruction of One-Dimensional Dielectric Scatterers Using Differential Evolution and Particle Swarm Optimization, *IEEE Geoscience and Remote Sensing Letters* **6**(4) (Oct. 2009), 671–675.
[7] K.A. Michalski, Electromagnetic Imaging of Circular-Cylindrical Conductors and Tunnels Using A Differential Evolution Algorithm, *Microwave and Optical Technology Letters* **27**(5) (Dec. 2000), 330–334.
[8] W. Chien, C.H. Huang, C.C. Chiu and C.L. Li, Image Reconstruction for 2D Homogeneous Dielectric Cylinder Using FDTD Method and SSGA, *International Journal of Applied Electromagnetics and Mechanics* **32**(2) (Feb. 2010), 111–123.

[9] S. Zhang, S.-X. Gong, Y. Guan, P.-F. Zhang and Q. Gong, A Novel IGA-EDSPSO Hybrid Algorithm for the Synthesis of Sparse Arrays, *Progress In Electromagnetic Research* **PIER 89** (2009), 121–134.

[10] W.-T. Wang, S.-X. Gong, Y.-J. Zhang, F.-T. Zha, J. Ling and T. Wan, Low RCS Dipole Array Synthesis Based on MoM-PSO Hybrid Algorithm, *Progress In Electromagnetic Research*, PIER 94, 2009, pp. 119–132.

[11] W. Chien, C.H. Huang and C.C Chiu, Cubic-Spline expansion for a Two-Dimensional Periodic Conductor in Free Space, *International Journal of Applied Electromagnetics and Mechanics* **24**(1–2) (Nov. 2006).

[12] C.C. Chiu and C.S. Ho, Image Reconstruction of a Two-Dimensional Periodic Conductor by the Genetic Algorithm, *Journal of Electromagnetic Waves and Applications* **15**(9) (Sept. 2001), 1175–1188.

[13] R.E. Jorgenson and R. Mittra, Efficient calculation of free-space periodic Green's function, *IEEE Trans. Antenna Propagat* **38** (May 1990), 633–642.

[14] G.S. Wallinga, E.J. Rothwell, K.M. Chen and D.P. Nyquist, Efficient computation of the two-dimensional periodic Green's function, *IEEE Tran. Antenna Propagat* **47** (May 1999), 895–897.

[15] S. Boutami and M. Fall, Calculation of Free-Space Periodic Green's Function Using Equivalent Finite Array, *IEEE Transactions on Antennas and Propagation* **60** (2012), 4725–4731.

[16] D. Van Orden and V. Lomakin, Rapidly Convergent Representations for Periodic Green's Functions of a Linear Array in Layered Media, *IEEE Transactions on Antennas and Propagation* **60**(2) (2012), 870–879.

[17] M. Clerc, The swarm and the queen: Towards a deterministic and adaptive particle swarm optimization, *Proceedings of Congress on Evolutionary Computation*, Washington, DC, 1999, pp. 1951–1957.

[18] J. Brest, S. Greiner, B. Boskovic, M. Mernik and V. Zumer, Self-adapting control parameters in differential evolution: comparative study on numerical benchmark problems, *IEEE Transactions on Evolutionary Computation* **10**(6) (Dec. 2006), 646–657.

[19] S.K. Goudos, K. Siakavara, T. Samaras, E.E. Vafiadis and J.N. Sahalos, Self-Adaptive Differential Evolution Applied to Real-Valued Antenna and Microwave Design Problems, *IEEE Transactions on Antennas and Propagation* **59**(4) (Apr. 2011), 1286–1298.